Research on Effects of Reynolds Number on Airfoil Flow Transition Position and Aerodynamic Characteristics by Calculation and Experiment

WANG Fei[1,2], *ZHANG Wei*[1*], *CHEN Xiaotian*[1]

1. China Helicopter Research and Development Institute, Jingdezhen 333000, P. R. China;
2. Jingdezhen Bamboo-Copter Aviation Technology Co., Ltd., Jingdezhen 333000, P. R. China

(Received 12 May 2025; revised 21 August 2025; accepted 29 December 2025)

Abstract: A flow transition prediction method for calculating effects of Reynolds numbers on aerodynamic characteristics of airfoil is developed, and the accuracy of the method is verified by wind tunnel experiment data and other calculation results. On these basics, the infrared thermal imager experiment results of the flow transition in low-speed wind tunnel and the aerodynamic characteristics experiment results with variable Reynolds number in high-speed wind tunnel are carried out respectively, and compared with the numerical results of helicopter rotor airfoil. Specially, effects of Reynolds numbers on airfoil aerodynamic characteristics by means of flow transition under different working conditions are researched and some meaningful conclusions are obtained. The calculation method, experiment method and results as well as the flow transition analysis conclusions for aerodynamic characteristics can be used for the design of helicopter rotor airfoil, especially for the helicopters under the high altitude and low Reynolds number working conditions.

Key words: helicopter rotor airfoil; Reynolds number; flow transition; aerodynamic characteristics

CLC number: V221.3 **Document code:** A **Article ID:** 1005-1120(2026)01-0015-12

0 Introduction

Thanks to the capability of vertical takeoff and landing, the helicopter can be used at high-altitude regions and in the areas with complex topography, such as Qinghai Tibet Plateau in southwest China. Known as the roof of the world, Qinghai Tibet Plateau has an average altitude above 4 000 m and even above 6 000 m for some ridges. For helicopters specially used on such regions, the required high-altitude performance is more stringent than the other ones in plain areas.

As the key rotating part of a helicopter, the rotor needs to provide thrust and control force in full flight envelope. As the basis of rotor blade aerodynamic layout design, airfoil aerodynamic characteristics, especially the drag characteristic, have a great impact on the performance of the rotor, which determines the useful payload and flight speed. As pointed out in Ref.[1], one factor determining the success of a new lifting rotor is the utilization of especially designed airfoils with aerodynamic features that well meet conditions of flow over the blade. Besides, with the increase of altitude, the engine power decreases significantly. Reducing rotor drag by maintaining laminar flow over a large portion of a rotor blade is a research hotspot. The difficulty of this research is the position prediction of airfoil flow transition.

Flow transition is one of the most important frontier problems in aerodynamics. Since the transition process is also affected by the turbulence of the flow, the Mach number, the pressure gradient and many other factors[2-3], there is a lack of unified un-

*Corresponding author, E-mail address: zhangw047@avic.com.

How to cite this article: WANG Fei, ZHANG Wei, CHEN Xiaotian. Research on effects of Reynolds number on airfoil flow transition position and aerodynamic characteristics by calculation and experiment[J]. Transactions of Nanjing University of Aeronautics and Astronautics, 2026, 43(1): 15-26.

http://dx.doi.org/10.16356/j.1005-1120.2026.01.002

derstanding of the transition mechanism. As a result, it is difficult to accurately predict flow transition through numerical calculation or to capture transition through experiments. Under varying altitudes, the blade profile has different Reynolds numbers, and the airfoil flow transition will be different. Therefore, it is necessary to establish the numerical method and experimental techniques for the calculation and capturing of flow transition, which consider the effects of Reynolds numbers. And the airfoil aerodynamic characteristics at low Reynolds numbers should be studied.

In Ref.[4], the relationship between helicopter flight performance and airfoil laminar flow is analyzed and the high-altitude airfoil is designed for the compound helicopter. Based on the example performance calculations, the high-altitude airfoil design requirements are estimated and the airfoils are designed. The design of a highly reflexed inboard airfoil enables the use of more camber over outboard sections. This allowed the working section airfoil to be designed for significant runs of laminar flow. The tip airfoil was designed for low drag at zero lift. Results were compared with existing rotorcraft airfoils over the high-altitude design space. In Ref.[5], the ability of three different methods to predict the lift, drag, and pitching moment coefficients of rotorcraft airfoils at the onset of dynamic stall is explored. It is quite widely understood that the proper prediction of transition is essential for an accurate prediction of the drag and the maximum lift coefficient. The aerodynamic characteristics of NACA0012 airfoil under different turbulence intensities and Reynolds numbers are simulated and compared with the experimental data. It shows that the flow characteristics of the airfoil with high turbulence or Reynolds number are more stable, and the separation bubble size is smaller[6]. Kong et al.[7] established a computational method suitable for analyzing dynamic stall of rotor airfoils in low-speed flow fields. They conducted computational analyses of the flow field characteristics of deep stall at different Mach numbers in low-speed conditions, demonstrating that the Mach number has a significant and regular influence on the hysteresis characteristics of dynamic stall.

The experimental data are summarized to study the effects of Reynolds number on airfoils with different thick[8]. Universal scaling laws and easily implemented methods are developed to account for Reynolds number effects in helicopter rotor analyses.

A variety of techniques have been developed for the detection of boundary layer transition but the applicability of these techniques varies with the experimental environment. A disadvantage of these techniques is that they all require surface coatings or electrical sensors, and these requirements can only be fulfilled in dedicated measurement campaigns with specially prepared blades[9-11].

In 2014, high-speed infrared thermography was applied to measure the boundary layer transition on the upper side of BO-105 helicopter rotors[12]. The measured transition characteristics are presented and compared with two-dimensional numerical simulations, and a good consistency is shown. The transition characteristics of EC135 helicopter rotor are measured by the same method and the effects of the contamination of the rotor blade leading edge on the laminar flow are discussed[12]. The differential infrared thermography was applied to detect the unsteady laminar/turbulent boundary layer transition of the NACA0012 airfoil in Ref.[13]. The measurements are compared with the numerical results, which are calculated by the DLR-TAU code with the Spalart-Allmaras turbulence model[14] together with the e^N transition prediction method[15].

Different from the previous researches, by combining numerical methods and wind tunnel experiments, the effects of Reynolds numbers on rotor airfoil flow transition are studied at low-speed and high-speed flow conditions. The mechanism of Reynolds number's effects on airfoil's aerodynamic characteristics is obtained, and it will support the theoretical analyses and technical design of rotor airfoil to meet the special environmental requirements of high plateau.

1 Establishment and Verification of Transition Numerical Simulation Method

In order to accurately carry out the research of airfoil flow transition calculation, a numerical simu-

lation method which can accurately simulate flow transition needs to be established and verified.

The Navier-Stokes equation considering viscosity and flow separation caused by viscosity is used as the governing equation[16-17], and the Gauss theorem is used to conduct space integration on control body element V, shown as

$$\frac{\partial}{\partial t}\iiint_V \boldsymbol{Q}\mathrm{d}V+\iint_S \boldsymbol{f}\cdot\boldsymbol{n}\mathrm{d}S=0 \tag{1}$$

where $\boldsymbol{Q}$ represents the conserved quantities, $\boldsymbol{f}$ the flux through the surface S with normal vector $\boldsymbol{n}$, and V the volume surrounded by S.

The finite volume method is used to discretize the equations. The MUSCL scheme[18] is used to solve the interpolation of state variables on the interface of elements, and the implicit approximate factorization method is used for time-marching. In order to better simulate flow separation, a k-ω shear stress transport (SST) two-equation model with transition and shear models is introduced[19].

Factors affecting airfoil aerodynamic characteristics are various and the influencing mechanism is complex. One of the mainly influence factors is the air flow state surrounding the airfoil, which can be divided into the laminar flow and the turbulence flow. Due to the significantly different friction drag, laminar or turbulent flow has significant influence on the drag. As a result, in the numerical calculation, the flow transition must be considered, and the flow transition regions must be accurately judged. At present, the main methods for predicting transitions in engineering include the transition empirical relation, the e^N method and the transition model method based on turbulence model theory. In order to improve the calculation accuracy, Langtry et al.[20-21] jointly proposed a transition model based on the local variables of the flow field in the SST turbulence model. The model combines the advantages of transition empirical relation and low Reynolds number turbulence model, and can predict transition more accurately.

Considering both grid generation efficiency and computational accuracy, a C-type mesh is employed in the computation, as shown in Fig.1, where c is the blade chord length.

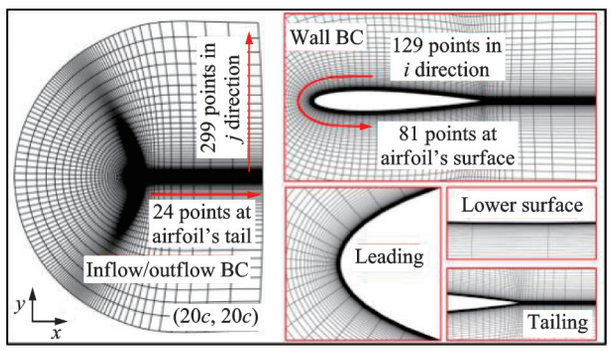

Fig.1 Structured grid of NACA 0012 airfoil

First, the grid independence was verified by comparing numerical and experimental aerodynamic results for the NACA 0012 airfoil at Ma=0.3 and Re=3.7×10^6 with varying grid resolutions. The grid resolutions are given in Table 1.

Table 1 Varying grid resolutions

Grid resolution	Number of grid points
Coarse	248 × 95
Medium	306 × 112
Fine	421 × 142

Fig.2 shows the comparison of the lift coefficient C_l and drag coefficient C_d under varying grid resolution α. As can be seen from Fig.2, the established aerodynamic analysis method demonstrates good agreement with experimental data in predicting

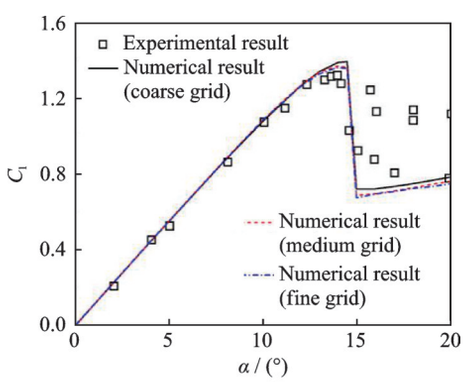

(a) Comparison of lift coefficient

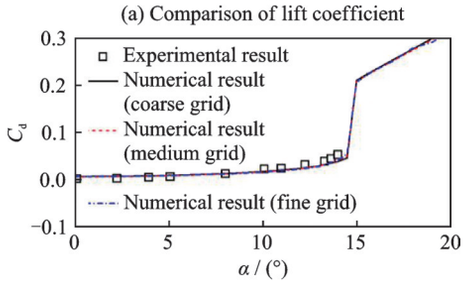

(b) Comparison of drag coefficient

Fig.2 Comparison of computational results under varying grid resolution

both the stall angle of attack and the linear region of lift. Additionally, the computed drag and pitching moment before stall exhibit excellent consistency with experimental measurements. Furthermore, the results obtained from different grid resolutions are nearly identical, indicating satisfactory grid convergence. The medium grid resolution is used in the following computations.

In order to test the accuracy of the numerical simulation method established in this paper for transition position prediction of airfoil flow, the transition position of NACA0012 airfoil is simulated. The simulation condition is the same with the experimental state of NACA0012 airfoil in Ref.[22], which is Ma=0.15 and Re=3×10^6. The calculated transition position, experimental results and numerical results in Ref.[16] are listed in Table 2. It can be seen that compared to the calculation results in Ref.[16], the calculation results in this paper are closer to the experimental results. The transition positions of both the upper and lower surfaces of airfoil are in better agreement with the experimental values, especially at the condition of high angle of attack.

Table 2 Transition position prediction of NACA0012 airfoil

α/(°)	Upper surface of airfoil			Lower surface of airfoil		
	Exp.	Ref.[16]	Cal.	Exp.	Ref.[16]	Cal.
0	0.450	0.43	0.46	0.45	0.43	0.46
3	0.200	0.21	0.23	0.66	0.72	0.65
5	0.085	0.13	0.13	0.79	0.88	0.79
8	0.024	0.07	0.04	0.92	1.00	0.98
10	0.013	0.04	0.02	1.00	1.00	1.00

In order to compare and analyze accuracy of the present calculation results in detail, Fig.3 shows the comparison between the calculated friction drag coefficient C_f in Ref.[16] and in this paper at α=3°, where x is the distance from the airfoil leading edge on chord. From Table 2, both the calculated results in Ref.[16] and in this paper are in good agreement with the experiment values at α=3°. It can be seen that the calculation result curves in this paper are completely consistent with the distribution shape, numerical value and variation trend of friction drag in Ref.[16]. The correctness of the method in this paper is further confirmed. It can also be seen from Fig.3 that compared to the full turbulence calculation results, the friction by transition model is much smaller, especially on the lower surface. The flow on lower surface maintains a long laminar flow state, and the friction drag is significantly smaller than the results by full turbulence model. Therefore, it is important to consider flow transition to improve the calculation accuracy of airfoil drag.

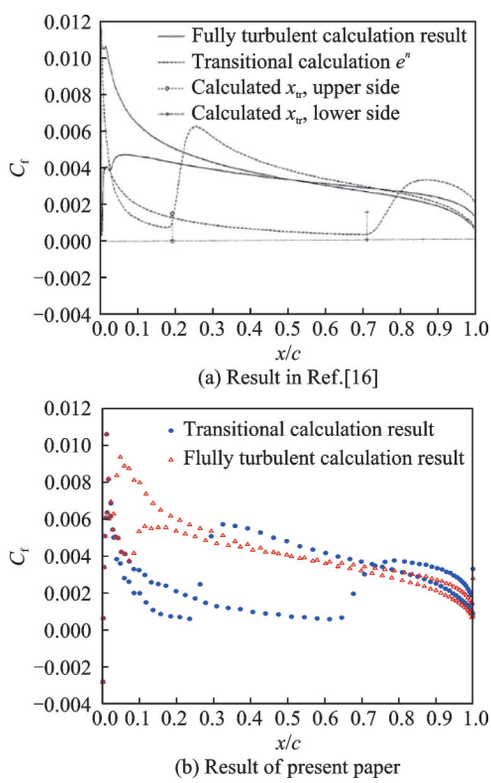

Fig.3 Friction drag comparison between Ref.[16] and present paper(α=3°)

Through comparative analysis, it can be concluded that the numerical simulation method in this paper can well simulate the transition of airfoil flow. The prediction of transition position and the friction drag values are highly accurate and reliable.

2 Flow Transition Calculation and Experimental Research for Special Rotor Airfoil

2.1 Transition experiment in low-speed wind tunnel

It is difficult to accurately capture the airfoil

flow transition position by experiment. In this paper, the infrared thermal imager is used to measure the flow transition position, by which the surface temperature of airfoil is measured. The measuring principle of the infrared thermal imager method is that the heat exchange generated by irregular pulsation in turbulence boundary layer is one order of magnitude higher than that in laminar boundary layer. If the surface temperature of an airfoil model has an obvious difference from the atmospheric temperature, it will step in flow transition region when the air flows through it. At the same time, for low speed incompressible flow, the surface temperature step can only be caused by the flow transition of the boundary layer. Therefore, the position of flow transition can be obtained by measuring the position of the temperature step on the airfoil surface using an infrared thermal imager. Due to the complexity of the experimental devices and the operation in the experiment process, this experiment is only suitable for the open-throat low-speed wind tunnel.

The experiment processes are as follows:

(1) Heat the surface of a special rotor airfoil model in the wind tunnel using a high-power electric heating plate, until the temperature reaches the expected value.

(2) Turn off the heating device power and remove it. Then, drive the wind tunnel at the same time.

(3) Collect the temperature field data of the airfoil model after the wind speed is stabilized.

(4) Determin the transition region through the images captured by the infrared thermal imager.

Two states of the airfoil at $Ma=0.2$, $\alpha=2^\circ$ and $Ma=0.2$, $\alpha=3^\circ$ ($Re=2.26\times10^6$) are experimentally measured, as shown in Figs.4, 5. And the results in Fig.4(a) and Fig.5(a) show that: at $\alpha=2^\circ$, the transition starting position is $x/c=0.22$, and the transition ending position is $x/c=0.27$. The dimensionless length of the transition region is 0.05. At $\alpha=3^\circ$, the transition starting position is $x/c=0.18$, and the transition ending position is $x/c=0.23$. The dimensionless length of the transition region is also 0.05.

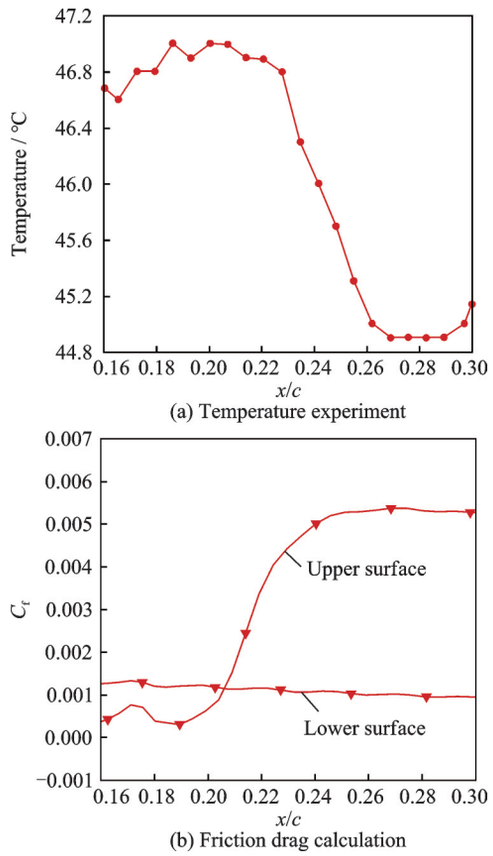

Fig.4 Experimental and calculation results for transition position ($Ma=0.2$, $\alpha=2^\circ$, $Re=2.26\times10^6$)

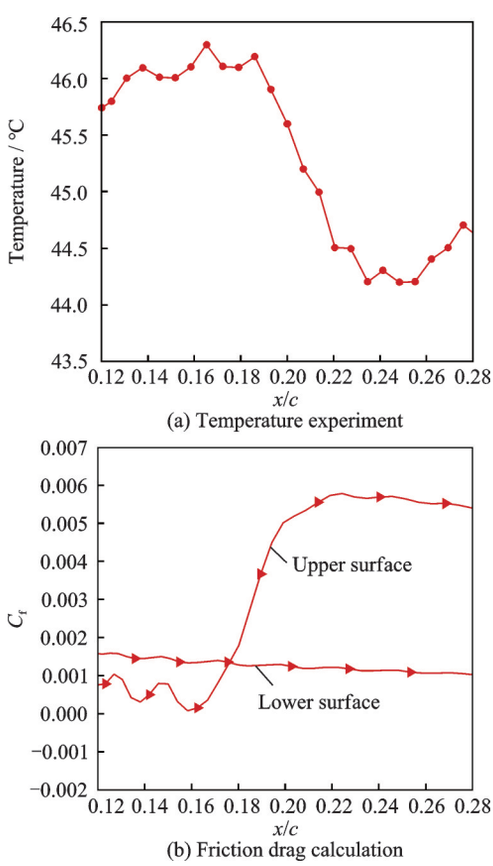

Fig.5 Experimental and calculation results for transition position ($Ma=0.2$, $\alpha=3^\circ$, $Re=2.26\times10^6$)

The experimental results show that the turbulent flow of the airfoil model has been fully developed at low speed and low angle of attack, such as at $Ma=0.2$, $\alpha=2^\circ$ and 3°. With the increase of angle of attack, the transition region moves forward as a whole, but the length of the transition region remains essentially unchanged.

2.2 Calculation and experiment results

Because the friction drag of the laminar boundary layer is much smaller than that of the turbulent boundary layer, the transition position can be predicted by monitoring the step change point of friction drag on the airfoil surface during the numerical simulation of the airfoil flow.

The calculation states are the same as the airfoil infrared thermal imager experiment states mentioned above. The calculation results in Fig.4(b) and Fig.5(b) show that: at $\alpha=2^\circ$, the transition starting position is $x/c=0.22$ and the ending position is $x/c=0.27$. The dimensionless length of the transition region is 0.06. At $\alpha=3^\circ$, the transition starting position is about $x/c=0.185$ and the ending position is $x/c=0.23$. The dimensionless length of the transition region is 0.05.

Comparing the calculation results and the experimental results, it is found that the calculation results of the transition region are slightly ahead of experimental results by 2% chord length, and the lengths of the transition regions are similar. The calculation results and the wind tunnel experiment results can be used to confirm each other. It is fully proved that the infrared thermal imager experiment method for the low-speed flow transition is reliable and the calculation method in this paper is accurate.

2.3 Calculation and analysis of the Reynolds number effect on low-speed flow transition

Based on the accurate numerical simulation and wind tunnel experimental research of the airfoil flow transition, the comparative analysis of effects of the angle of attack and the Reynolds number on airfoil flow transition is carried out by the established method. Fig.6 shows the surface friction drag of the airfoil at different angles of attack under $Re=1.13\times10^6$ and $Re=2.26\times10^6$, respectively. Similarly, the flow transition region can be predicted by comparing and analyzing the step of friction drag on airfoil surface.

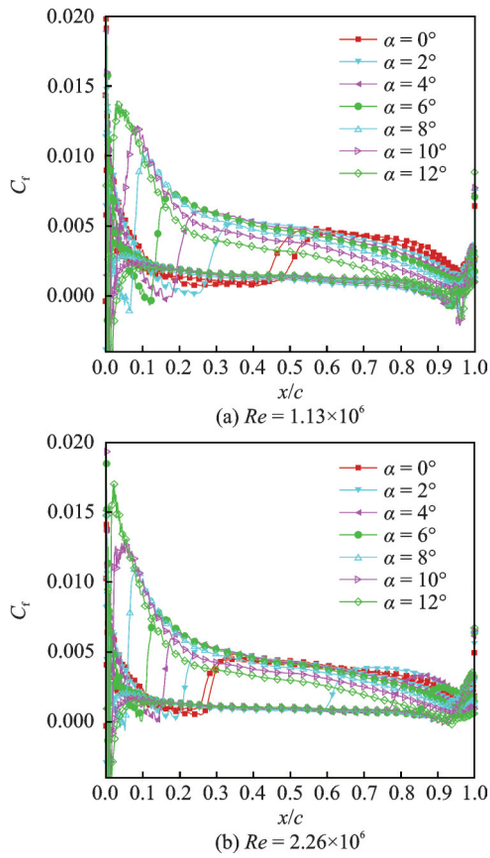

Fig.6 Comparison of friction drag of a helicopter rotor airfoil under different Reynolds numbers at different angles of attack

Table 3 shows the specific transition starting positions, the ending positions, and the length of the transition regions obtained by identifying the step of airfoil surface friction drag from Fig.6. The calculation results are analyzed as follows.

Table 3 Transition region prediction (x/c) of a helicopter rotor airfoil

α/(°)	$Re=1.13\times10^6$			$Re=2.26\times10^6$		
	Start	End	Region	Start	End	Region
0	0.43	0.57	0.14	0.250	0.320	0.070
2	0.26	0.37	0.11	0.200	0.260	0.060
4	0.18	0.25	0.07	0.140	0.190	0.050
6	0.12	0.17	0.05	0.100	0.130	0.030
8	0.07	0.11	0.04	0.052	0.077	0.025
10	0.04	0.07	0.03	0.013	0.023	0.010
12	0.01	0.03	0.02	0.008	0.016	0.008

(1) Influence of different angles of attack at the same Reynolds number

At the same Reynolds number, with the increase of the angle of attack, the transition starting position gradually moves to the leading edge of the airfoil. Under the condition of low angle of attack, the transition region is wider and the turbulence is not fully developed. With the increase of angle of attack, the transition region gradually decreases. That is, the transition region is compressed and gradually moves forward. The laminar flow area gradually shrinks, and the turbulence region gradually expands until it diffuses to the leading edge of the airfoil, fully covering the airfoil surface.

(2) Influence of different Reynolds numbers at the same angle of attack

Compared to the results under $Re=1.13\times10^6$, the flow transition position moves forward obviously and the transition region shrinks under $Re=2.26\times10^6$ with the same angle of attack. Moreover, even at the state of low angle of attack, the transition from laminar flow to turbulence can also be achieved.

2.4 Comparative research on high-speed wind tunnel experiment and calculation

For the high-speed wind tunnel experiment of a special rotor airfoil, it should be carried out in the transonic wind tunnel. Experiments on the effects of Reynolds numbers on airfoil aerodynamic characteristics are conducted at atmospheric pressure (one atmospheric pressure) and pressurization (two atmospheric pressures), respectively. For this airfoil, the experiment conditions are $Ma=0.7$ and $Re=2.6\times10^6$, 5.2×10^6, respectively. The experimental results and the corresponding numerical calculation results of C_l and C_d at different Reynolds numbers are shown in Figs.7, 8.

In wind tunnel experiments, lift coefficients are obtained by measuring the pressure distribution on the airfoil surface. It can be seen that the lift coefficients in the linear segment are very consistent under different Reynolds numbers. However, at the condition of high angle of attack, the lift curve slope under the pressurized state is slightly larger. In addition, according to the calculation results, the airfoil under the pressurized state has a larger stall angle of attack and a larger maximum lift coefficient. The experiment and calculation results of the lift coefficient

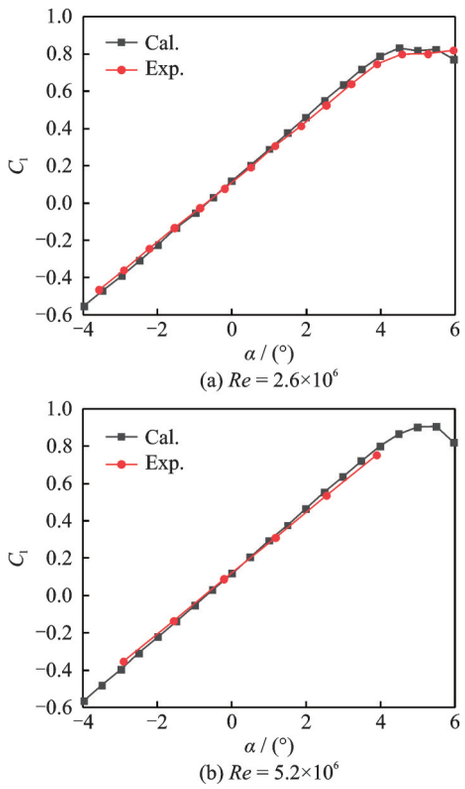

Fig.7 Lift coefficient at different Reynolds numbers

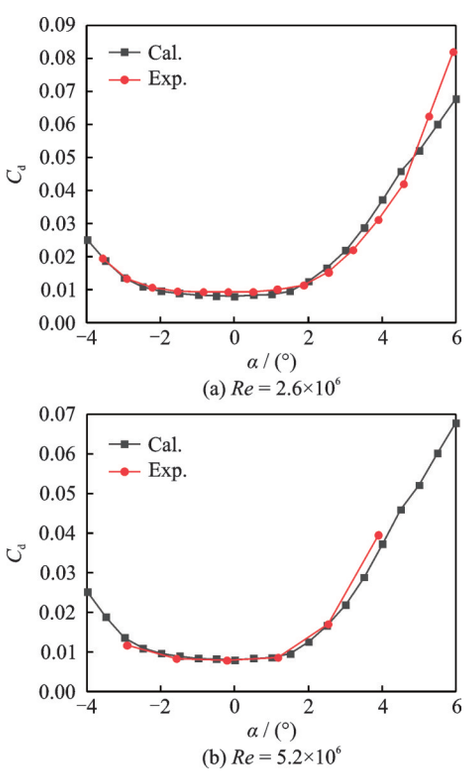

Fig.8 Drag coefficient at different Reynolds numbers

show good consistency and conform to the general law of the influence of the Reynolds number on aerodynamic characteristics. And, the drag coefficients of the airfoil are obtained by measuring the total pressure loss in the wake area of the airfoil flow field and converting it into momentum loss, expressed as Eqs.(2, 3). The total pressure loss in the wake is measured by a wake row-tube, on which 53 total pressure measuring tubes and four static pressure measuring tubes are arranged.

$$C_d = \int_{-h/2}^{h/2} C_f(y)\frac{dy}{c} - C_{dwt} \tag{2}$$

$$C_f = 2\cdot\left(\frac{P_w}{P_\infty}\right)^{\frac{1}{\gamma}}\cdot\left(\frac{P_{0,w}}{P_0}\right)^{\frac{\gamma-1}{\gamma}}\cdot\sqrt{\frac{\left[1-\left(\frac{P_w}{P_{0,w}}\right)^{\frac{\gamma-1}{\gamma}}\right]}{\left[1-\left(\frac{P_\infty}{P_0}\right)^{\frac{\gamma-1}{\gamma}}\right]}}\cdot\left(1-\sqrt{\frac{\left[1-\left(\frac{P_\infty}{P_{0,w}}\right)^{\frac{\gamma-1}{\gamma}}\right]}{\left[1-\left(\frac{P_\infty}{P_0}\right)^{\frac{\gamma-1}{\gamma}}\right]}}\right) \tag{3}$$

where h is the height of wake row-tube, $P_{0,w}$ the total pressure measured at the wake, P_w the average value of static pressure measured by the static pressure tubes on the wake row-tube, C_{dwt} the drag coefficient caused by the flow loss of wind tunnel, and $\gamma=1.4$.

Analyzing the wind tunnel experiment and calculation results of drag coefficient, it is found that both of them show the general law[23] that the drag decreases when the Reynolds number increases at a small angle of attack (-2°—$+2^\circ$). The corresponding physical meaning is that the increased Reynolds number decreases effects of the viscosity and the friction drag. However, as the angle of attack increases, the drag coefficient under the pressurization state gradually exceeds that under the atmospheric pressure state, namely, with the increase of the Reynolds number, the drag increases. In addition, experimental results and numerical calculation results of the wind tunnel show the same phenomenon, which is different from the general influence trend of the Reynolds number on drag. And, a more detailed analysis is conducted.

In order to further analyze the reasons for the increase of drag when the Reynolds number is increased, Fig.9 shows the comparisons of pressure coefficient C_p on airfoil surface at $\alpha=1.17^\circ$, 2.54°, and 3.90° under the atmospheric pressure ($Re=2.6\times10^6$) and pressurization wind tunnel experiments ($Re=5.2\times10^6$). For $\alpha=1.17^\circ$, the pressure distribution on the airfoil surface is basically the same at atmospheric pressure and pressurization condition, and the negative pressure peak of the airfoil leading edge is slightly wider under pressurization condition. For $\alpha=2.54^\circ$, the basic pattern of the airfoil surface pressure distribution remains unchanged for both atmospheric pressure and pressurization condition, while the negative pressure peak of the airfoil leading edge remains longer under pressurized condition. For $\alpha=3.90^\circ$, the airfoil surface pressure distribution of atmospheric basic pattern still remains unchanged. The negative pressure peak on airfoil leading edge under pressurization condition becomes narrow, and a decrease phenomenon of pressure drop gradient appears, which means the speed reduction rate decreases.

Fig.10 shows the comparison of drag coefficient distributions at $Ma=0.7$, $\alpha=1.17^\circ$, 2.54°, and 3.90° at the atmospheric pressure and pressurization by wake measurement. At different angles of attack, the drag peaks in atmospheric pressure and pressurized state are basically the same. The difference is that the drag distribution pattern measured in pressurized state is "fatter" than that in atmospheric pressure state when $\alpha=2.54^\circ$ and 3.90°. Since the drag distribution measured by the wake is a comprehensive performance of various factors, the wind tunnel experiment can only find the abnormal phenomenon that the drag at a high Reynolds number is larger than that at a low Reynolds number in some states of the airfoil, but the specific reasons cannot be given from the flow details or flow mechanism.

Further, the distribution diagrams of friction drag on the airfoil surface are obtained by calculation and presented in Fig.11. From Fig.11, we can draw the following conclusions.

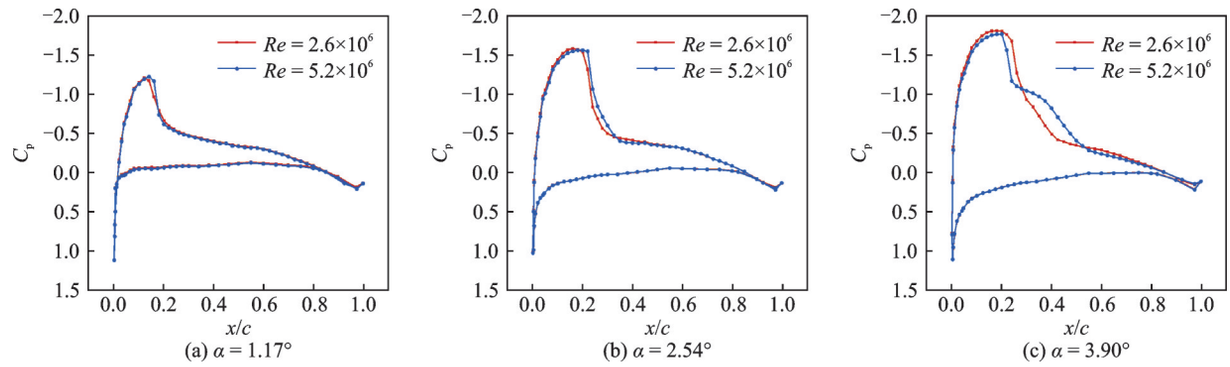

Fig.9 Airfoil surface pressure distribution at different Reynolds numbers

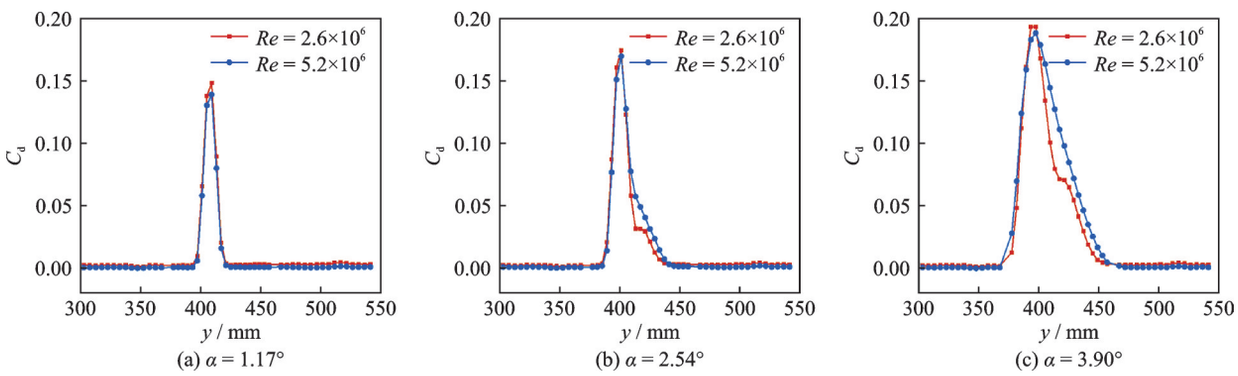

Fig.10 Drag distribution by wake total pressure experiment at different Reynolds numbers

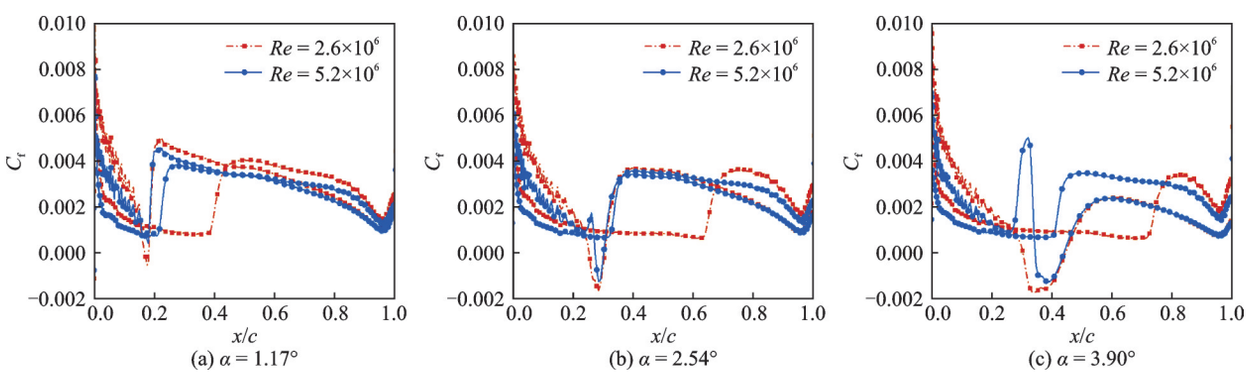

Fig.11 Friction drag distribution on airfoil surface at different Reynolds numbers

(1) When $\alpha=1.17°$ and $Re=2.6\times10^6$, a very small separation bubble appears near $x/c=0.175$ and then rapidly reattaches to the airfoil surface, and flow transitions appear at the same time. However, at $Re=5.2\times10^6$, no flow separation bubbles appear, although flow transition also occurs on the upper surface of the airfoil at almost the same position. Because the flow separation occurs at a low Reynolds number, the friction drag at a low Reynolds number is relatively greater in both laminar flow section and turbulence section. And thus, at this angle of attack, the drag of airfoil at a low Reynolds number is greater.

(2) When $\alpha=2.54°$, at both Reynolds numbers, flow separation bubbles appear on the airfoil upper surface near $x/c=0.285$, and then rapidly attach to the airfoil surface, followed by flow transition. On the airfoil's lower surface, flow transition occurs later at $Re=2.6\times10^6$, and most of the flow area is laminar. At $Re=5.2\times10^6$, flow transition on the lower surface occurs earlier, almost at the same x/c station position as on the upper surface. Therefore, at a high Reynolds number, the airfoil is covered by turbulence in a larger area than at a low Reynolds number, resulting in a larger airfoil drag at high Reynolds number.

(3) At $\alpha=3.90^{\circ}$ and $Re=5.2\times10^{6}$, on the airfoil upper surface, flow transition takes place firstly near $x/c=0.284$, followed by the formation of separation bubbles near $x/c=0.38$. At $Re=2.6\times10^{6}$, a relatively larger separation bubble is generated in a slightly forward position. After bubble separation, flow transitions occur under both Reynolds numbers. On the lower surface of airfoil, flow transition occurs later at $Re=2.6\times10^{6}$, and most of the area is laminar flow. At $Re=5.2\times10^{6}$, flow transition occurs earlier, almost at the same x/c station as the upper surface. At a high Reynolds number, flow transition occurs first and then flow separates on the upper surface of the airfoil. And the transition position of the lower surface is earlier than that at the lower Reynolds number. These two factors together lead to greater drag of the airfoil at a high Reynolds number. The corresponding airfoil flow field distribution is shown in Fig.12, where y is the local airfoil thickness.

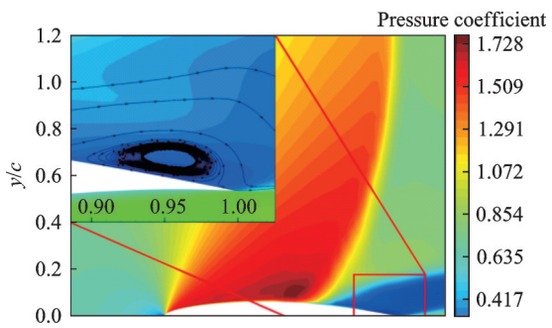

Fig.12 Airfoil flow field distribution

3 Conclusions

In this paper, a high precision numerical method for airfoil aerodynamic characteristics calculation, which considers the flow transition effect, is established and verified. The results show that the numerical method can accurately calculate airfoil drag and capture flow transition. Based on the method, comparative research on the effects of Reynolds numbers on the aerodynamic characteristics of special rotor airfoils at low-speed and high-speed is carried out by numerical calculation and wind tunnel experiment. Some significant results are obtained for the personalized airfoil design of the helicopter used in special environments. The main conclusions are as follows:

(1) Comparative analysis of numerical calculation results and infrared thermal imager experiment results proves the feasibility and accuracy of flow transition measurement by infrared thermal imager experiment method in low-speed flow, effectively solving the problem of flow transition measurement.

(2) The margin of error of flow transition position between experiment and numerical prediction is within 2% chord.

(3) In low-speed flow, Reynolds number has a significant effect on the airfoil transition position. For the working environment of the helicopter rotor airfoil, the inner section of the blade basically works in the state of low-speed flow and large angle of attack. Therefore, it is necessary to pay special attention to the changes in transition position and transition region caused by the Reynolds number, so as to accurately improve the rotor performance.

(4) The aerodynamic characteristics of the airfoil, especially the drag characteristics, do not always conform to the general law that the drag decreases with the increase of the Reynolds number. In some states, due to the influence of the Reynolds number on transition or flow separation, the drag may increase with the increase of the Reynolds number.

(5) The results show that the design of helicopter airfoils should not only consider the aerodynamic characteristics of airfoils at standard atmosphere and sea level, but also should examine the aerodynamic characteristics at high altitude and low Reynolds number conditions. Especially for China's unique high plateau operating environment, it is necessary to carry out research and design of plateau rotor airfoils based on high plateau and low Reynolds number design points.

References

[1] BOUSMAN W G. Airfoil design and rotorcraft performance[C]//Proceedings of American Helicopter Society 58th Annual Forum. Montreal, Canada: American

Helicopter Society, 2002.

[2] RESHOTKO E. Boundary-layer stability and transition[J]. Annual Review of Fluid Mechanics, 1976, 8: 311-349.

[3] MOIN P, MAHESH K. Direct numerical simulation: A tool in turbulence research[J]. Annual Review of Fluid Mechanics, 1998, 30(1): 539-578.

[4] MARTIN P B. Rotor blade airfoil design for high-altitude, long-endurance VTOL UAVs[C]//Proceedings of American Helicopter Society UAV Specialist Meeting. [S.l.]: American Helicopter Society, 2005.

[5] VIEIRA B A O, MAUGHMER M D. An evaluation of dynamic stall onset prediction methods for rotorcraft airfoil design[C]//Proceedings of the 51st AIAA Aerospace Sciences Meeting Including the New Horizons Forum and Aerospace Exposition. Grapevine, Texas: AIAA, 2013: AIAA2013-1093.

[6] ZHANG Yang, ZHOU Zhou, LI Xu. Effect of turbulence intensity and gradient of turbulence intensity on airfoil aerodynamic characteristics at low Reynolds number[J]. Journal of Northwestern Polytechnical University, 2021, 39(4): 721-730. (in Chinese)

[7] KONG Weihong, CHEN Renliang, SUN Zhenhang. Numerical investigation of dynamic stall on rotor airfoil in low-speed flow[J]. Journal of Nanjing University of Aeronautics & Astronautics, 2018, 50(2): 213-220. (in Chinese)

[8] YAMAUCHI G K, JOHNSON W. Trends of Reynolds number effects on two-dimensional airfoil characteristics for helicopter rotor analyses: NASA 83N24472[R]. [S.l.]: NASA, 1983.

[9] TANNER W H, YAGGY P F. Experimental boundary layer study on hovering rotors[J]. Journal of the American Helicopter Society, 1966, 11(3): 22-37.

[10] RAFFEL M, DE GREGORIO F, DE GROOT K, et al. On the generation of a helicopter aerodynamic database[J]. The Aeronautical Journal, 2011, 115(1164): 103-112.

[11] YORITA D, ASAI K, KLEIN C, et al. Transition detection on rotating propeller blades by means of temperature-sensitive paint: AIAA—2012-1187[R]. [S.l.]: AIAA, 2012.

[12] DLR G A C, RICHTER K, SCHÜLEIN E. Boundary layer transition measurements on hovering helicopter rotors by infrared thermography[C]//Proceedings of the Vertical Flight Society 70th Annual Forum. Montréal, Québec: The Vertical Flight Society, 2014: 1-13.

[13] KAI R, MERZ C, RAFFEL M. Unsteady boundary layer transition measurements by differential infrared thermography[C]//Proceedings of the Vertical Flight Society 70th Annual Forum. Montréal, Québec: The Vertical Flight Society, 2014: 1-9.

[14] SPALART P R, ALLMARAS S R. A one-equation model for aerodynamic flows: AIAA 92-0439[R]. Reno, NV, USA: AIAA, 1992.

[15] DRELA M. Newton solution of coupled viscous/inviscid multielement airfoil flows[C]//Proceedings of the 21st Fluid Dynamics, Plasma Dynamics and Lasers Conference. Seattle, WA, USA: AIAA, 1990.

[16] ZAK M. Correction to Euler's equations and elimination of the closure problem in turbulence[J]. AIP Advances, 2012, 2(4): 042123.

[17] BLAZEK J. Computational fluid dynamics: Principle and applications[M]. 2nd ed. [S.l.]: Elsevier , 2005.

[18] VAN LEER B. Towards the ultimate conservative difference scheme. V: A second-order sequel to Godunov's method[J]. Journal of Computational Physics, 1979, 32(1): 101-136.

[19] MENTER F R. Two-equation eddy-viscosity turbulence models for engineering applications[J]. AIAA Journal, 1994, 32(8): 1598-1605.

[20] LANGTRY R B, MENTER F R, LIKKI S R, et al. A correlation based transition model using local variables, Part 1—Model formulation: ASME 2004-GT-53452[R]. [S.l.]: ASME, 2004.

[21] LANGTRY R B, MENTER F R, LIKKI S R, et al. A correlation based transition model using local variables Part 2—Test cases and industrial applications: ASME 2004-GT-53434[R]. [S.l.]: ASEM, 2004.

[22] JOHANSEN J, SØRENSEN J N. Prediction of laminar/turbulent transition in airfoil flows[J]. Journal of Aircraft, 1999, 36(4): 731-734.

[23] WANG Shicun. Helicopter aerodynamics[M]. Beijing, China: Science Press, 2024. (in Chinese)

Authors

The first author Dr. **WANG Fei** received his Ph.D. degree in flight vehicle design from Nanjing University of Aeronautics and Astronautics, in 2018. Afterwards, he was employed at China Helicopter Research and Development Institute as an engineer. His current research interests include helicopter aerodynamics and noise reduction design.

The corresponding author Prof. **ZHANG Wei** received his M.S. degree in engineering mechanics from Northwestern Polytechnical University, Xi'an, China. He is currently a researcher-level senior engineer and performs research in the field of rotorcraft design.

Author contributions Dr. **WANG Fei** designed the study, compiled the models, conducted the analysis, and wrote the manuscript. Prof. **ZHANG Wei** contributed to the data and model components for the model. Mr. **CHEN Xiaotian** revised the manuscript and contributed to the numerical simulation. All authors commented on the manuscript draft and approved the submission.

Competing interests The authors declare no competing interests.

(Production Editor: ZHANG Huangqun)

基于转捩的雷诺数对翼型气动特性影响计算与实验研究

王 菲[1,2], 张 威[1], 陈笑天[1]

(1.中国直升机设计研究所,景德镇 333000,中国; 2.景德镇竹蜻蜓航空科技有限责任公司,景德镇 333000,中国)

摘要:层流向湍流的转捩一直是流体力学中最重要的前沿问题之一。本文发展了计入流动转捩的雷诺数对翼型气动特性影响计算分析方法,并就该方法对流动转捩预测的准确性进行了风洞试验数据和计算结果的验证。基于此,针对直升机旋翼专用翼型,分别开展了低速风洞流动转捩红外热像仪测量实验、高速风洞变雷诺数翼型气动特性实验和计算结果对比研究,并有针对性地研究了在不同工况下雷诺数通过影响流动转捩对翼型气动特性的不同影响结果。研究发现,相同的雷诺数下随迎角增大,翼型的流动转捩起始点逐渐向翼型前端移动,且翼型转捩区间随迎角增大逐渐减小。此外,翼型阻力并非永远都是随着雷诺数增大而减小,部分状态因为雷诺数对流动转捩或者流动分离的影响,导致可能存在随着雷诺数增大阻力增大的现象。所建立的翼型气动特性计算方法、实验方法和结果以及流动转捩分析结果可为中国直升机旋翼专用翼型设计,特别是高高原、低雷诺数工况下使用的旋翼专用翼型研究和设计提供参考。

关键词:直升机旋翼翼型;雷诺数;转捩;气动特性

研究亮点:

1. 建立了一种基于转捩模型的翼型气动特性方法,其能够更好地适用于高高原直升机旋翼翼型转捩特性预测及气动性能评估。

2. 开展了低速风洞流动转捩红外热像仪测量实验、高速风洞变雷诺数翼型气动特性实验,并和计算结果进行了对比。结果证明在低速流动中用红外热像仪实验方法测量流动转捩的可行性和准确性,有效解决流动转捩测量难的问题。

3. 有针对性地研究了在不同工况下雷诺数通过影响流动转捩对翼型气动特性的不同影响结果。研究发现,雷诺数对翼型的气动特性,特别是阻力特性,并非永远都是符合随着雷诺数增大而阻力减小的一般规律,部分状态因为雷诺数对流动转捩或者流动分离的影响,导致可能存在随着雷诺数增大阻力增大的现象。